THE JOURNAL OF PHYSICAL CHEMISTRY C

Article

pubs.acs.org/JPCC

Indium Tin Oxide Nanowire Networks as Effective UV/Vis Photodetection Platforms

Songqing Zhao,[†,‡] Daniel Choi,[†] Thomas Lee,[†] Anthony K. Boyd,[§] Paola Barbara,[§] Edward Van Keuren,[§] and Jong-in Hahm*[,†]

[†]Department of Chemistry, Georgetown University, 37th & O Streets NW, Washington, DC 20057, United States

[‡]College of Science, China University of Petroleum, Beijing 102249, People's Republic of China

[§]Department of Physics, Georgetown University, 37th & O Streets NW, Washington, DC 20057, United States

ABSTRACT: We demonstrate that indium tin oxide nanowires (ITO NWs) and cationic polymer-modified ITO NWs configured in a network format can be used as high performing UV/vis photodetectors. The photovoltage response of ITO NWs is much higher than similarly constructed devices made from tin oxide, zinc tin oxide, and zinc oxide nanostructures. The ITO NW mesh-based devices exhibit a substantial photovoltage (31−100 mV under illumination with a 1.14 mW 543 nm laser) and photocurrent (225−325 μA at 3 V). The response time of the devices is fast with a rise time of 20−30 μs and a decay time of 1.5−3.7 ms when probed with a 355 nm pulsed laser. The photoresponsivity of the ITO NW devices ranges from 0.07 to 0.2 A/W at a 3 V bias, whose values are in the performance range of most commercial UV/vis photodetectors. Such useful photodetector characteristics from our ITO NW mesh devices are attained straightforwardly without the need for complicated fabrication procedures involving highly specialized lithographic tools. Therefore, our approach of ITO NW network-based photodetectors can serve as a convenient alternative to commercial or single NW-based devices.

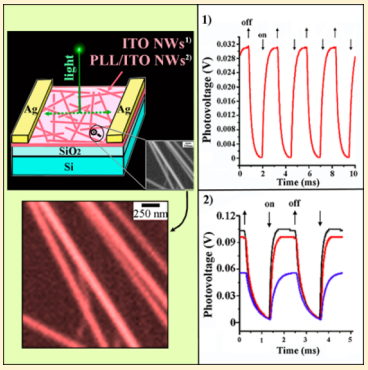

INTRODUCTION

One-dimensional (1D) semiconducting nanomaterials have proven their promising potential in crucial sensing applications by serving as chemical, biological, and light sensors.[1−4] In particular, transparent conducting oxide (TCO) nanostructures have shown their versatility in sensing various types of analytes ranging from gas species to biological molecules to light.[1−4] The improved performance leading to increased signal and fast response time is often attributed to the inherently high surface-to-volume ratio of nanomaterials, when compared to the same sensing devices which are made from thin film or bulk structures.

Both individual nanostructures and their ensembles have been previously employed to construct sensor devices. Typical fabrication processes involving individual nanostructures require the use of high-cost, low-yield, and highly specialized fabrication equipment, presenting challenges for scalability of their assembly and production. On the other hand, sensors constructed from networks of nanostructures are not subjected to the complicated fabrication processes often employed for single nanostructure devices, potentially enabling a large-scale production via facile and low-cost techniques. Nanostructure network devices may also benefit from better light trapping and suppressed reflection.[5,6] In addition to these advantages, ensemble platforms have shown to provide adequate or improved performances,[7−9] making them very attractive, alternative sensor devices that are easy to fabricate. Significant research efforts have so far been made to characterize single TCO nanostructure devices. Yet, it is equally important to examine nanomaterial network devices, when considering the aforementioned overall effectiveness of sensor devices constructed from nanomaterial ensembles. In this regard, we have previously demonstrated the different uses of indium tin oxide nanowire (ITO NW) network systems in biomolecular fluorescence and surface-enhanced Raman signal detection.[10,11]

Here we examine ITO NW network devices for photosensor applications. We demonstrate that ITO NW network-based devices can function as highly effective photodetectors capable of sensing ultraviolet (UV) and visible (VIS) light with high sensitivity and fast response time. We also show that the UV/vis sensing capability of the ITO NW mesh devices can be significantly improved by modifying the NWs with a cationic polymer, poly-L-lysine. High photovoltage and photocurrent signals are observed from these sensors, with much faster rise and decay time than those reported for single NW devices. The photoresponsivity of the ITO NW mesh devices is comparable to those of commercial UV/vis detectors even at a low bias. In addition, our ITO NW mesh-based devices are fabricated with simple processes which do not involve lithographic patterning or thin film deposition. Therefore, our approach can be highly beneficial to developing alternative platforms for low-cost, high performing photodetectors with improved scalability.

Special Issue: Steven J. Sibener Festschrift

Received: June 18, 2014
Revised: August 11, 2014
Published: August 21, 2014

   dx.doi.org/10.1021/jp506074c | J. Phys. Chem. C 2015, 119, 14483−14489

EXPERIMENTAL SECTION

Silicon wafers (resistivity <1 Ω cm, thickness: 0.017 in.) and Au colloid (20 nm in diameter) were obtained from Silicon Quest International Inc. (Santa Clara, CA) and Ted Pella, Inc. (Redding, CA), respectively. A Si wafer with a thin layer of Au catalysts was then placed approximately 5 in. downstream from a 2:1 mixture of graphite and ITO powder (In_2O_3:SnO_2 = 90:10 wt %) which was kept at the center of a home-built chemical vapor deposition (CVD) reactor. The sample was subsequently produced in the horizontal resistance furnace under a constant flow of 100 standard cubic centimeters per minute (sccm) of Ar, similar to the process reported earlier[10] at the reaction temperature of 850 °C for 15 min. Other nanostructures of tin oxide (SnO_2), zinc tin oxide (ZTO), and zinc oxide (ZnO) were similarly produced for photovoltage comparison with ITO. They were generated by using a 1:1 mixture of graphite and SnO_2 heated to 850 °C for 2 h, a 5:1 mixture of graphite and ZTO powder (SnO_2:ZnO = 50:50 wt %) at 915 °C for 10 min, and a 2:1 mixture of graphite and ZnO heated to 900 °C for 1 h, respectively. As-grown nanostructures form a thin layer on the Si supports. The size and morphology of CVD-synthesized nanomaterials were then characterized by using a FEI/Philips XL 20 scanning electron microscope (SEM) operated at 20 kV. X-ray diffraction (XRD) data were acquired by using a Rigaku Ultima IV X-ray diffractometer (The Woodlands, Texas) operated with an accelerating voltage and current of 45 kV and 44 mA, respectively, under Cu K_α radiation. The samples were scanned at a rate of 2°/min in the range of 2θ = 5−80°.

Ag contacts were fabricated using silver pastes (Ted Pella, Inc.) on either end of the nanomaterial layer serving as the left (L) and right (R) electrodes for subsequent, lateral photovoltage (LPV) measurements. The sample assembly was then placed in a dark housing with a small front aperture to introduce a light source to the sample while eliminating any external optical and electrical noise. At the bottom center of the enclosure, a sample holder connects the two electrodes on the sample to the 200 MHz oscilloscope through a BNC connector for voltage characterization. A 543 nm HeNe laser (Newport Corp., Santa Clara, CA) was used as a constant-wave, visible (VIS) illumination source, with a spot diameter and laser power of 1 mm and 1.14 mW, respectively. The light was sent through an optical chopper (Thorlabs, Inc., Newton, NJ) rotating with a predetermined frequency. UV illumination was delivered by a Quanta-Ray GCR-3 pulsed Nd:YAG laser (Spectra Physics, Santa Clara, CA) as a light source. The frequency-tripled output of the laser (wavelength 355 nm) has a measured pulse width of 8 ns, repetition rate of 10 Hz, and maximum pulse energy of 200 mJ. The beam was attenuated to give a pulse energy of roughly 15 μJ per pulse incident on the sample with a spot size of 1 mm. In addition, current−voltage (I−V) measurements were carried out by sweeping the L−R voltage using a Hewlett-Packard pA-meter/DC-voltage source, HP 4140B.

RESULTS AND DISCUSSION

Figure 1(a) displays representative 4 × 4 μm SEM panels for as-grown SnO_2, ZTO, ZnO, and ITO nanomaterials. Nanowire (NW)-like structures are observed from SnO_2 and ITO plates, whereas nanorod (NR) and nanobelt (NB) structures are found from the ZnO and ZTO plates, respectively. The average diameter of SnO_2 NWs (35.7 ± 2.0 nm) is similar to that of

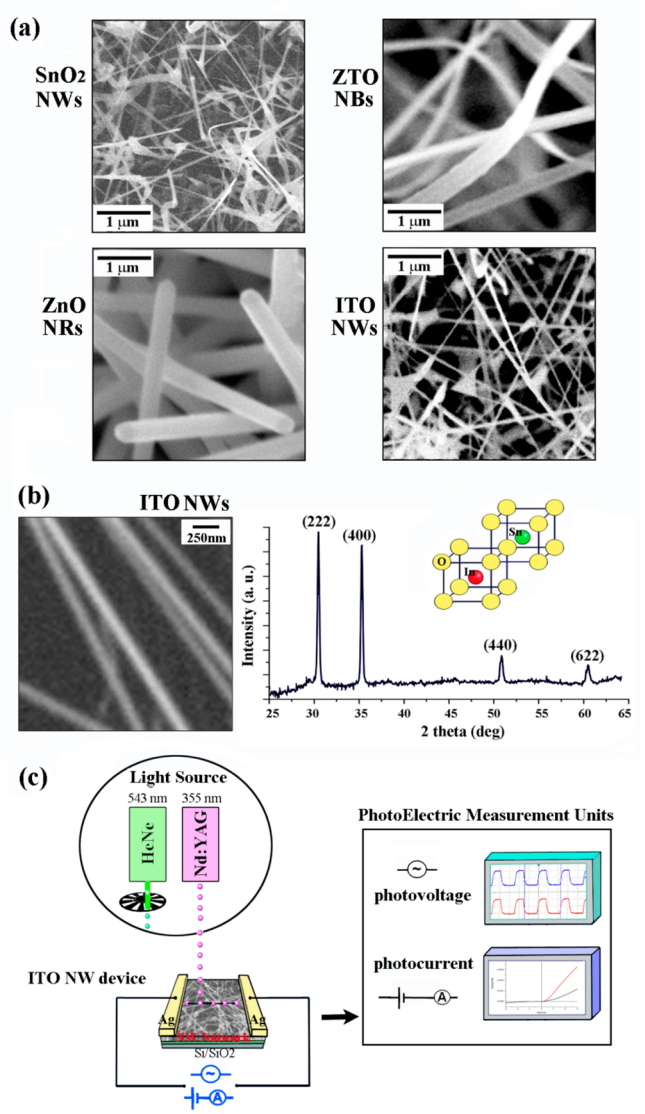

Figure 1. (a) 4 × 4 μm SEM images displaying typical CVD-grown structures of SnO_2 NWs, ZTO NBs, ZnO NRs, and ITO NWs. (b) A 2 × 2 μm, zoomed-in SEM panel shows the structure of individual ITO NWs. XRD data of as-grown ITO NWs are also provided along with a schematic representation of the atomic arrangements in ITO NW crystals. (c) Schematic diagram of our overall photoelectric measurement setup.

ITO NWs (40 ± 1.5 nm), whereas the diameter of ZTO NBs (333 ± 45 nm) is similar to that of ZnO NRs (300 ± 15 nm). Figure 1(b) shows a magnified SEM panel and X-ray diffraction (XRD) data of ITO NWs, the material of focus in this paper. XRD peaks positioned at 30.45°, 35.28°, 50.80°, and 60.40° correspond to (222), (400), (440), and (622) ITO NW planes in the cubic crystal structure of bixbyite Mn_2O_3 I type (C-type rare-earth oxide structure), respectively. The atomic arrangements of In, Sn, and O in the ITO NWs are depicted in the crystal structure model provided in Figure 1(b). Our overall experimental scheme for the nanomaterial network photoelectric measurements is displayed in Figure 1(c).

The device schematic provided in Figure 2(a) displays a typical sample configuration involving networks of ITO NWs. Figure 2(a) also displays a representative voltage response obtained from ITO NWs, showing a maximum photovoltage (V_{ph}) value of 31 mV. Down (up) arrows inserted in Figure 2

dx.doi.org/10.1021/jp506074c | J. Phys. Chem. C 2015, 119, 14483−14489

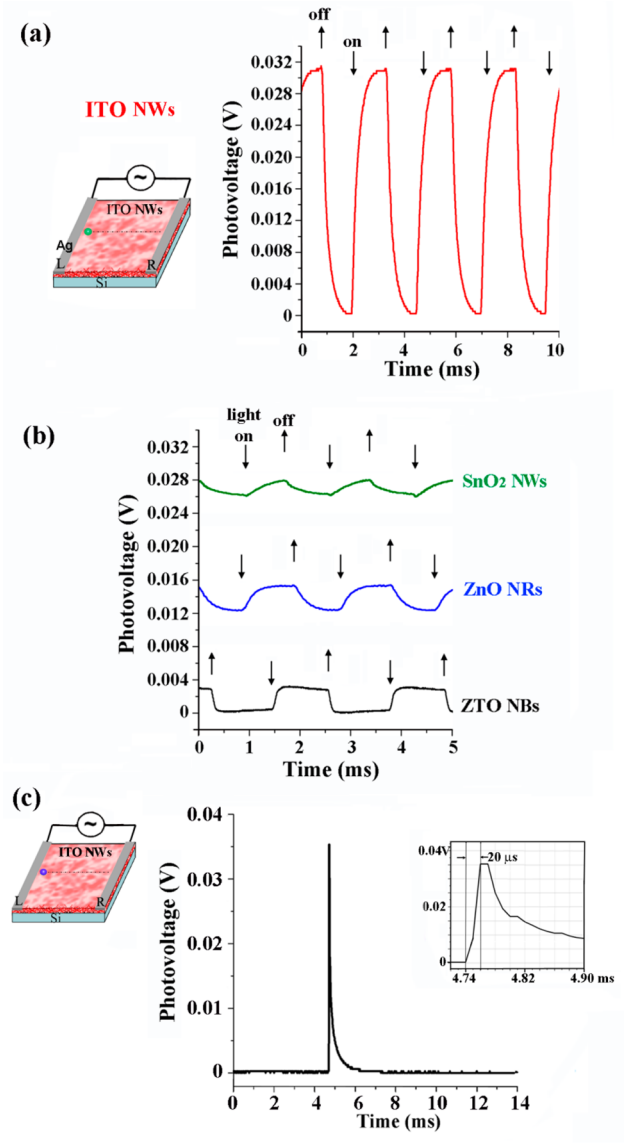

Figure 2. (a) Typical photovoltage acquired from ITO NWs while illuminating the device with a 543 nm laser through an optical chopper is shown. (b) Photovoltage signal from SnO_2, ZTO, and ZnO nanostructures is recorded when using the same light source as (a). (c) Typical photovoltage signal obtained from ITO NW devices when using a 355 nm pulsed laser is provided. The inset is a zoomed-in view with the light on to show clearly the rise time.

indicate the time when the 543 nm laser directed to the sample is on (off) through a 400 Hz chopper wheel. In comparison, Figure 2(b) displays typical photovoltage plots acquired from the other three types of devices consisting of SnO_2 NWs, ZnO NRs, and ZTO NBs. The voltage responses upon illumination on these materials are significantly lower than what we observe from ITO NWs. Both ZnO NR and ZTO NB devices result in V_{ph} of ~3 mV, whereas SnO_2 NWs produce an even weaker signal of ~2 mV. Although the exact origin of the increased photovoltage response observed from ITO NWs in comparison to other nanomaterials is not clear yet, various inherent electrical properties of the materials, such as charge carrier density, resistivity, and carrier mobility, may contribute to this effect. The corresponding values for an ITO thin film, for example, are, respectively, reported to be on the order of $5 \times 10^{20}/cm^3$, 2×10^{-4} Ω·cm, and 55 $cm^2/(V \cdot s)$,[12,13] whereas those of a ZnO thin film are $10 \times 10^{19}/cm^3$, 1×10^{-2} Ω·cm, and 35 $cm^2/(V \cdot s)$.[14] The higher charge carrier density and mobility combined with the lower resistivity of ITO may promote the enhanced photoinduced voltage signal in our experiment. The magnitude of V_{ph} varies on the same sample devices depending on the laser position. The laser spot is kept on the sample location, producing the highest signal for all devices characterized in Figure 2. When comparing the highest V_{ph} of the different devices, the photoresponse of ITO NWs is an order of magnitude larger than other similar semiconducting oxide nanomaterials shown in Figure 2(b). Therefore, herein we focus our discussion of this paper on ITO NWs. The response time of the photovoltage change of the ITO NW device is determined by using the pulsed Nd:YAG laser as a light source. Figure 2(c) displays the typical response time of the ITO NW photodetectors which is defined collectively by the rise (T_r) and decay (T_d) time. The response time of ITO NW devices is determined as T_r = 20 μs and T_d = 1.5 ms.

Electrical responses in many nanomaterial-based electronic devices can be effectively tailored by a simple modification of the channel surfaces of the devices.[15−19] Organic amines and polymers have been utilized previously as gates or gate modifiers in chemical- and electrolyte-gating applications, respectively.[15−19] These methods can produce a large change in electrical signal via simple means without introducing chemical dopants or charge-separating layers into the channel material. In order to test whether the light-activated, electrical response of our nanomaterial devices can be altered in a similar way, a cationic polymer of PLL was chosen as a model system and uniformly applied to the surface of the ITO NW layer. Typical photovoltage signals from the PLL-treated ITO NW (PLL/ITO NW) devices were subsequently probed by using the 543 nm laser, and the results are provided in Figure 3(a). When keeping the same laser spot on the sample position yielding the highest signal, a significantly increased V_{ph} value of 100 mV is recorded on PLL/ITO NWs as plotted in black in Figure 3(a). The photoresponse decreases when it is positioned away from the edge toward the middle of the sample. Colored plots in Figure 3(b) display such changes in photoresponse amplitudes when varying the laser position along a line spanning from one electrode to the other (marked as L and R electrodes in the schematics) on the PLL/ITO NW device. V_{ph} varies with the light position on the line between the L and R electrodes with $\Delta V_{ph}/\Delta x$ of approximately 20 mV/mm for PLL/ITO NWs. Figure 3(c) displays the photovoltage response of the PLL/ITO NW device upon illumination with the 355 nm pulsed laser. The response time of the PLL/ITO NW device is slightly longer than the ITO NW device, exhibiting T_r = 30 μs and T_d = 3.7 ms.

As the excitation wavelengths of both lasers used in our experiments are below the bandgap of ITO NWs[20] (>3.75 eV), the photoresponse is not due to the generation of charge carriers from bandgap transition. One possible cause for the photovoltage is local heating in the region of the ITO NW network irradiated by the laser. It is known that light-induced temperature gradients in single and ensemble nanomaterials can produce a photovoltage through photothermoelectric effect (PTE) in a carbon nanotube, graphene, MoS_2, and GaAs NW devices.[21−27] Upon illumination, there will be a net electrical current from the hot side to the cold side until the electric field build-up balances this current. When the laser spot is positioned on one side of the network, close to one contact, the photovoltage is highest since the net current from the one

dx.doi.org/10.1021/jp506074c | J. Phys. Chem. C 2015, 119, 14483−14489

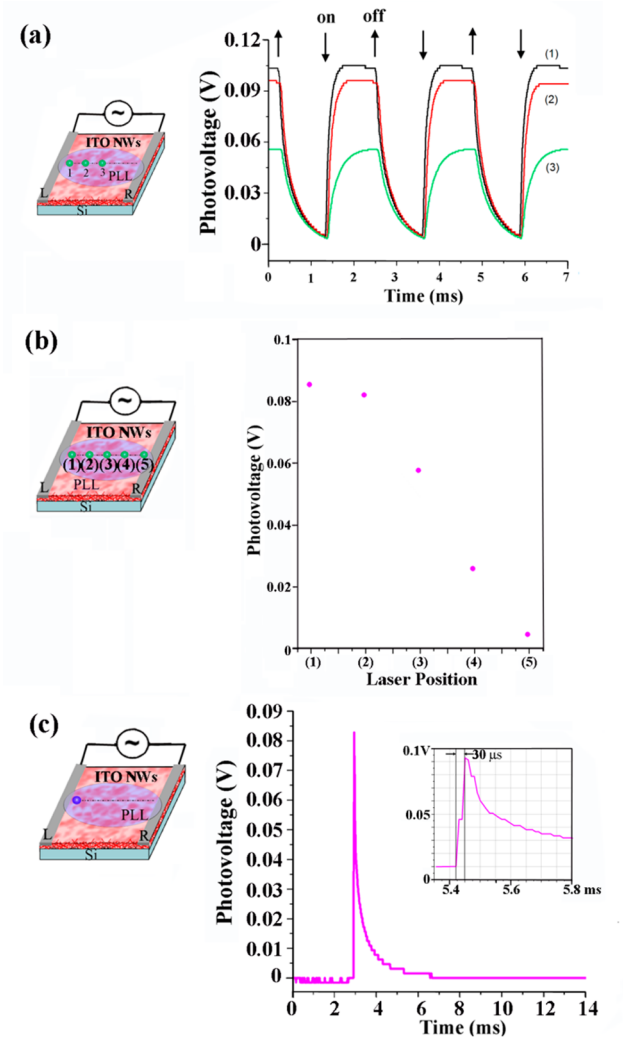

Figure 3. (a) Typical photovoltage response obtained from PLL-modified ITO NW devices upon periodic illumination with a 543 nm laser displayed. Plots indicated as (1), (2), and (3) correspond to voltage signal changes depending on the laser position as indicated in the schematic. (b) Voltage difference ($V_{ph} - V_d$) between 543 nm light-on and -off is recorded at five different illumination positions along the middle of the PLL/ITO NW device spanning one electrode to the other. Relative laser positions are marked as (1) through (5) as shown in the schematic. (c) Typical photovoltage signal obtained from PLL/ITO NW devices probed by a 355 nm pulsed laser is shown. The inset is a zoomed-in view with the light on to show clearly the rise time.

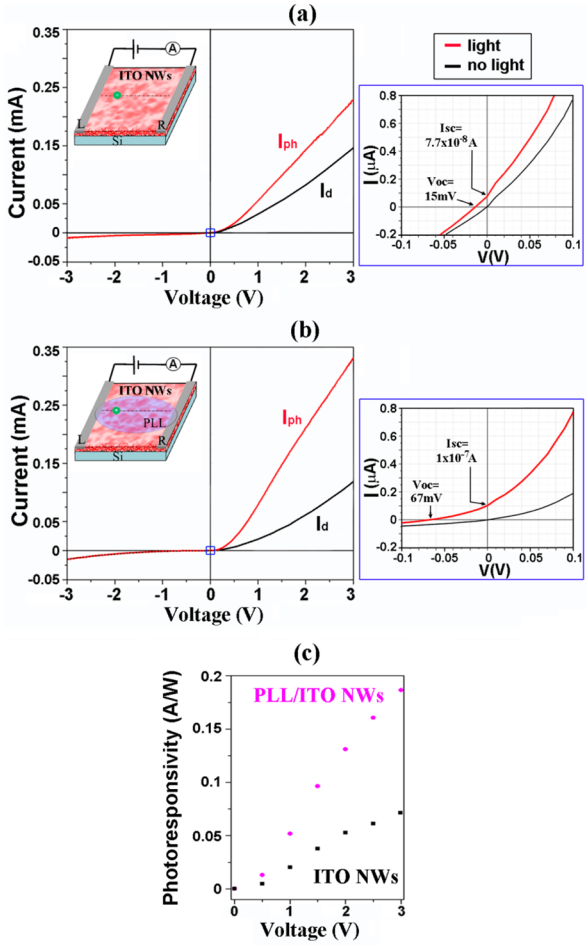

Figure 4. (a) Typical current versus voltage ($I-V$) plot is shown for ITO NWs. Dark current (I_d) and photocurrent (I_{ph}) are obtained while sweeping the L−R voltage from −3 to +3 V. The 543 nm laser serves as the illumination source. The $I-V$ plot in the right panel displays a magnified view of the blue squared region in the $I-V$ curve on the left. The open-circuit voltage (V_{oc}) and short-circuit current (I_{sc}) upon illumination are determined as 15 mV and 7.7×10^{-8} A, respectively, for the ITO NWs. (b) Typical $I-V$ characteristics are displayed for PLL/ITO NW devices. The open-circuit voltage (V_{oc}) and short-circuit current (I_{sc}) upon illumination are determined as 67 mV and 1.0×10^{-7} A, respectively, as indicated in the magnified $I-V$ panel shown on the right. (c) The photoresponsivity data of the ITO NW and PLL/ITO NW mesh devices are plotted against the bias in black and purple, respectively.

contact (on the hot side) to the other contact (on the cold side) will be largest. When the laser spot is moved close to the middle of the sample, the current caused by the temperature gradient will flow from the hot middle region in both directions toward the two colder contacts, yielding a smaller net photovoltage. Therefore, for a symmetric device, photovoltage should be zero when the laser is positioned in the middle. Our results shown in Figure 3(b) indicate an asymmetric device behavior, yielding a nonzero photovoltage at all five laser positions tested.

In order to understand this response, current−voltage ($I-V$) measurements were carried out by sweeping the L−R voltage from −3 to 3 V with an increment of 10 mV using the HP pA-meter/DC-voltage source. The light source used for the $I-V$ measurements was the 543 nm laser. Figure 4 displays the resulting $I-V$ characteristics of the ITO NW devices with and without the PLL modification. Asymmetric $I-V$ curves are observed from both ITO NW and PLL/ITO NW devices. Such asymmetrical $I-V$ curves have been reported previously on single nanomaterial devices such as ZnO NBs and NWs as well as Ge NW mesh devices.[28−31] However, the exact origin of the rectifying $I-V$ curves in these systems is not clear and still under debate.

Surface charge- and oxygen adsorbate-driven mechanisms often explaining photocurrent transport behaviors of many single NW devices will lead to a much slower reset time than what we observe from ITO NW-based devices. This slow response time of single NW devices is due to a long time scale associated with surface trap charging and the oxygen read-sorption process (several minutes to hours).[31,32] In contrast, the very fast response and decay time observed from our ITO

dx.doi.org/10.1021/jp506074c | J. Phys. Chem. C 2015, 119, 14483−14489

Table 1. Key Characteristics of UV/Vis Photodetectors Constructed from Various TCO Nanomaterials[a]

material type	λ_{light}	V	I_{ph}	T_r	T_d	ref
Co-ZnO NBs	370 nm	5 V	110 μA	200 s	-	37
	630 nm	5 V	0.25 μA	500 s	-	
ZnO NW	390 nm	5 V	30 μA	23 s	33 s	36
ZnO NW	350 nm	5 V	~0.01 μA	40 s	300 s	40
Au NP−ZnO NW	350 nm	5 V	~1 μA	25 s	10 s	40
SnO_2 NBs	532 nm	−5 V	57 nA	<1 s	<1 s	38
In_2O_3 NW	254 nm	0.3 V	290 nA	10 s	~900 s	39
	365 nm	0.3 V	33 nA	-	~300 s	
ITO NW mesh	355 nm	-	-	20 μs	1.5 ms	this study
	543 nm	3 V	225 μA	-	-	
PLL/ITO NW mesh	355 nm	-	-	30 μs	3.7 ms	this study
	543 nm	3 V	325 μA	-	-	

[a]Co-ZnO NB and SnO_2 NB devices contain ensembles of nanomaterials, whereas ZnO NW and In_2O_3 NW systems are examples of individual nanomaterial devices. Parameters such as bias voltage (V), photocurrent (I_{ph}), rise time (T_r), and decay time (T_d) are catalogued.

NW network devices in Figures 2(c) and 3(c) strongly suggest that a different mechanism may play a key role in our NW mesh configuration. We hypothesize that our devices are governed by a barrier-dominated transport mechanism. The L and R electrodes in our devices form different contact barriers at the interface with the ITO NW network due to variations in contact conditions caused by nonuniformity of the network, yielding asymmetric $I-V$ characteristics. At the same time, NW−NW junction barriers existing in the NW mesh configuration may also contribute to the asymmetry of the $I-V$ curves. The typical rise/decay time, on the order of micro-/milliseconds, observed from our ITO NW network devices indicates that photothermally induced charge carriers are instantaneously formed within tens of microseconds after illumination with the pulsed laser. However, such charge carriers can be restrained at the NW−NW interfaces and/or NW−Ag contact junctions, resulting in decay times in tens of milliseconds when the light is off. Hence, an alternative ITO device fabricated with aligned NWs between the two contacts may be able to reduce the time scale gap between the rise and decay time by minimizing the carrier trap at the NW−NW interfaces. Further work is underway to measure exactly the differences in the contact barriers at the NW−metal junctions in the L and R electrodes as well as to investigate the choice of metal for the electrodes.

The open circuit voltage (V_{oc}) and short circuit current (I_{sc}) were also obtained from the $I-V$ curves. These results are clearly seen in the zoomed-in $I-V$ plots of Figures 4(a) and 4(b) for the ITO NW and PLL/ITO NW device, respectively. Under the dark condition, no significant V_{oc} or I_{sc} is measured from the ITO NW or the PLL/ITO NW device. Upon illumination, the ITO NW device exhibits V_{oc} and I_{sc} of 15 mV and 7.7×10^{-8} A, respectively. These values change to V_{oc} = 67 mV and $I_{sc} = 1.0 \times 10^{-7}$ A for the PLL-modified ITO NW device under the same illumination condition. Figure 4(c) displays the photoresponsivity, $R = [(I_{ph} - I_d)/(P^*a)]$, of the ITO NW and PLL/ITO NW devices shown in Figures 4(a) and 4(b). I_{ph}, I_d, P, and a correspond to the photocurrent, dark current, power density of the laser, and the cross-sectional area of the illumination, respectively. When using the 543 nm laser, the ITO NWs reach the R value of 0.07 A/W at 3 V, whereas the PLL-treated ITO NWs display R = 0.2 A/W at the same bias. The typical photoresponsivity of most commercial UV and vis photodetectors is in the range of 0.1−0.2 and 0.1−0.5 A/W, respectively.[33−35] Hence, the photoresponsivity of our ITO NW mesh-based devices is comparable to the performance of commercial UV and vis photodetectors.

For comparison with other similar nanomaterial devices, Table 1 lists the performance characteristics of UV and vis photodetectors made from various individual and ensemble TCO nanomaterials.[36−39] Key parameters of the light sensors are also shown along with those of our ITO NW mesh-based devices. The high performing ITO NW mesh devices demonstrated in this study can be straightforwardly constructed without the use of intensive lithographic steps and, thus, can potentially enable a large-scale production of ITO NW-based, UV−vis photodetectors. At the same time, our ITO NW network devices display fairly high I_{ph} and R values even at a low bias of 3 V, while featuring a very fast response time of T_r and T_d.

CONCLUSIONS

In summary, we have shown that ITO NWs and PLL/ITO NWs configured in a network format can be effectively used as high performing UV/vis photodetectors. The photovoltage response of ITO NWs is much higher than similarly constructed devices made from SnO_2 NWs, ZTO NBs, and ZnO NRs. The ITO NW mesh-based devices yield substantial photovoltage and photocurrent values of 31−100 mV and 225−325 μA at 3 V, respectively, under illumination with a 1.14 mW, 543 nm laser. The photoresponsivity of the ITO NW devices ranges from 0.07 to 0.2 A/W at a 3 V bias. The response time of the devices exhibits a rise time of 20−30 μs and a decay time of 1.5−3.7 ms when probed with a 355 nm pulsed laser. These photodetectors are simple and straightforward to construct without the need of complicated fabrication steps involving highly specialized instrumentations. Therefore, our efforts demonstrate that ITO NW network-based photodetectors can serve as a convenient alternative to commercial or single NW-based devices as easily assembled, high performing photodetectors.

AUTHOR INFORMATION

Corresponding Author

*Phone: (202) 687-5950. E-mail: jh583@georgetown.edu.

Notes

The authors declare no competing financial interest.

■ ACKNOWLEDGMENTS

The authors acknowledge financial support on this work by the National Institutes of Health, National Research Service Award (1R01DK088016) from the National Institute of Diabetes and Digestive and Kidney Diseases, and by the National Science Foundation Grant (DMR-1008242). S.Z. and J.H. acknowledge the Georgetown University-Chinese Science Council (GU-CSC) postdoctoral program.

■ REFERENCES

(1) Xiang, J.; Lu, W.; Hu, Y.; Wu, Y.; Yan, H.; Lieber, C. M. Ge/Si Nanowire Heterostructures as High-Performance Field-Effect Transistors. *Nature* **2006**, *441*, 489−493.
(2) Law, M.; Goldberger, J.; Yang, P. D. Semiconductor Nanowires and Nanotubes. *Annu. Rev. Mater. Res.* **2004**, *34*, 83−122.
(3) Xia, Y.; Yang, P.; Sun, Y.; Wu, Y.; Mayers, B.; Gates, B.; Yin, Y.; Kim, F.; Yan, H. One-Dimensional Nanostructures: Synthesis, Characterization, and Applications. *Adv. Mater.* **2003**, *15*, 353−389.
(4) Hahm, J.-i. Biomedical Detection via Macro- and Nano-Sensors Fabricated with Metallic and Semiconducting Oxides. *J. Biomed. Nanotechnol.* **2013**, *9*, 1−25.
(5) Zhu, J.; Yu, Z.; Burkhard, G. F.; Hsu, C.-M.; Connor, S. T.; Xu, Y.; Wang, Q.; McGehee, M.; Fan, S.; Cui, Y. Optical Absorption Enhancement in Amorphous Silicon Nanowire and Nanocone Arrays. *Nano Lett.* **2008**, *9*, 279−282.
(6) Huang, Y.-F.; Chattopadhyay, S.; Jen, Y.-J.; Peng, C.-Y.; Liu, T.-A.; Hsu, Y.-K.; Pan, C.-L.; Lo, H.-C.; Hsu, C.-H.; Chang, Y.-H.; et al. Improved Broadband and Quasi-Omnidirectional Anti-Reflection Properties with Biomimetic Silicon Nanostructures. *Nat. Nanotechnol.* **2007**, *2*, 770−774.
(7) Unalan, H. E.; Zhang, Y.; Hiralal, P.; Dalal, S.; Chu, D.; Eda, G.; Teo, K. B. K.; Chhowalla, M.; Milne, W. I.; Amaratunga, G. A. J. Zinc Oxide Nanowire Networks for Macroelectronic Devices. *Appl. Phys. Lett.* **2009**, *94*, 163501.
(8) Cao, Q.; Kim, H.-s.; Pimparkar, N.; Kulkarni, J. P.; Wang, C.; Shim, M.; Roy, K.; Alam, M. A.; Rogers, J. A. Medium-scale Carbon Nanotube Thin-Film Integrated Circuits on Flexible Plastic Substrates. *Nature* **2008**, *454*, 495−500.
(9) Yan, C.; Singh, N.; Lee, P. S. Wide-Bandgap Zn_2GeO_4 Nanowire Networks as Efficient Ultraviolet Photodetectors with Fast Response and Recovery Time. *Appl. Phys. Lett.* **2010**, *96*, 053108.
(10) Kumar, N.; Parajuli, O.; Feng, M.; Xu, J.; Hahm, J.-i. Facile Fabrication and Biological Application of Tin-Rich Indium Tin Oxide Nanorods. *Appl. Phys. Lett.* **2010**, *96*, 053705.
(11) Zhao, S.; Guo, Y.; Song, S.; Choi, D.; Hahm, J.-i. Application of Well-Defined Indium Tin Oxide Nanorods as Raman Active Platforms. *Appl. Phys. Lett.* **2012**, *101*, 053117.
(12) Yasuhara, R.; Murai, S.; Fujita, K.; Tanaka, K. Atomically Smooth and Single Crystalline Indium Tin Oxide Thin Film with Low Optical Loss. *Phys. Status Solidi C* **2012**, *9*, 2533−2536.
(13) Bel Hadj Tahar, R.; Ban, T.; Ohya, Y.; Takahashi, Y. Tin Doped Indium Oxide Thin Films: Electrical Properties. *J. Appl. Phys.* **1998**, *83*, 2631−2645.
(14) Maragliano, C.; Lilliu, S.; Dahlem, M. S.; Chiesa, M.; Souier, T.; Stefancich, M. Quantifying Charge Carrier Concentration in ZnO Thin Films by Scanning Kelvin Probe Microscopy. *Sci. Rep.* **2014**, *4*, 1−7.
(15) Kong, J.; Dai, H. Full and Modulated Chemical Gating of Individual Carbon Nanotubes by Organic Amine Compounds. *J. Phys. Chem. B* **2001**, *105*, 2890−2893.
(16) Abdula, D.; Shim, M. Performance and Photovoltaic Response of Polymer-Doped Carbon Nanotube p−n Diodes. *ACS Nano* **2008**, *2*, 2154−2159.
(17) Panzer, M. J.; Frisbie, C. D. Polymer Electrolyte-Gated Organic Field-Effect Transistors: Low-Voltage, High-Current Switches for Organic Electronics and Testbeds for Probing Electrical Transport at High Charge Carrier Density. *J. Am. Chem. Soc.* **2007**, *129*, 6599−6607.
(18) Yuen, J. D.; Dhoot, A. S.; Namdas, E. B.; Coates, N. E.; Heeney, M.; McCulloch, I.; Moses, D.; Heeger, A. J. Electrochemical Doping in Electrolyte-Gated Polymer Transistors. *J. Am. Chem. Soc.* **2007**, *129*, 14367−14371.
(19) Ozel, T.; Gaur, A.; Rogers, J. A.; Shim, M. Polymer Electrolyte Gating of Carbon Nanotube Network Transistors. *Nano Lett.* **2005**, *5*, 905−911.
(20) Hamberg, I.; Granqvist, C. G. Evaporated Sn-Doped In_2O_3 Films: Basic Optical Properties and Applications to Energy-Efficient Windows. *J. Appl. Phys.* **1986**, *60*, R123.
(21) DeBorde, T.; Aspitarte, L.; Sharf, T.; Kevek, J. W.; Minot, E. D. Photothermoelectric Effect in Suspended Semiconducting Carbon Nanotubes. *ACS Nano* **2013**, *8*, 216−221.
(22) Withers, F.; Bointon, T. H.; Craciun, M. F.; Russo, S. All-Graphene Photodetectors. *ACS Nano* **2013**, *7*, 5052−5057.
(23) Buscema, M.; Barkelid, M.; Zwiller, V.; van der Zant, H. S. J.; Steele, G. A.; Castellanos-Gomez, A. Large and Tunable Photothermoelectric Effect in Single-Layer MoS_2. *Nano Lett.* **2013**, *13*, 358−363.
(24) St-Antoine, B. C.; Ménard, D.; Martel, R. Position Sensitive Photothermoelectric Effect in Suspended Single-Walled Carbon Nanotube Films. *Nano Lett.* **2009**, *9*, 3503−3508.
(25) Prechtel, L.; Padilla, M.; Erhard, N.; Karl, H.; Abstreiter, G.; Fontcuberta I Morral, A.; Holleitner, A. W. Time-Resolved Photoinduced Thermoelectric and Transport Currents in GaAs Nanowires. *Nano Lett.* **2012**, *12*, 2337−2341.
(26) Kim, M. H.; Yan, J.; Suess, R. J.; Murphy, T. E.; Fuhrer, M. S.; Drew, H. D. Photothermal Response in Dual-Gated Bilayer Graphene. *Phys. Rev. Lett.* **2013**, *110*, 247402.
(27) Wu, C.-C.; Jariwala, D.; Sangwan, V. K.; Marks, T. J.; Hersam, M. C.; Lauhon, L. J. Elucidating the Photoresponse of Ultrathin MoS_2 Field-Effect Transistors by Scanning Photocurrent Microscopy. *J. Phys. Chem. Lett.* **2013**, *4*, 2508−2513.
(28) Harnack, O.; Pacholski, C.; Weller, H.; Yasuda, A.; Wessels, J. M. Rectifying Behavior of Electrically Aligned ZnO Nanorods. *Nano Lett.* **2003**, *3*, 1097−1101.
(29) Lao, C. S.; Liu, J.; Gao, P.; Zhang, L.; Davidovic, D.; Tummala, R.; Wang, Z. L. ZnO Nanobelt/Nanowire Schottky Diodes Formed by Dielectrophoresis Alignment Across Au Electrodes. *Nano Lett.* **2006**, *6*, 263−266.
(30) Liao, Z.-M.; Xu, J.; Zhang, J.-M.; Yu, D.-P. Photovoltaic Effect and Charge Storage in Single ZnO Nanowires. *Appl. Phys. Lett.* **2008**, *93*, 023111.
(31) Yan, C.; Singh, N.; Cai, H.; Gan, C. L.; Lee, P. S. Network-Enhanced Photoresponse Time of Ge Nanowire Photodetectors. *ACS Appl. Mater. Interfaces* **2010**, *2*, 1794−1797.
(32) Zhai, T.; Fang, X.; Liao, M.; Xu, X.; Zeng, H.; Yoshio, B.; Golberg, D. A Comprehensive Review of One-Dimensional Metal-Oxide Nanostructure Photodetectors. *Sensors* **2009**, *9*, 6504−6529.
(33) Carey, J. E.; Crouch, C. H.; Shen, M.; Mazur, E. Visible and Near-Infrared Responsivity of Femtosecond-Laser Microstructured Silicon Photodiodes. *Opt. Lett.* **2005**, *30*, 1773−1775.
(34) Monroy, E.; Omnès, F.; Calle, F. Wide-Bandgap Semiconductor Ultraviolet Photodetectors. *Semicond. Sci. Technol.* **2003**, *18*, R33−R51.
(35) Geist, J.; Zalewski, E. F.; Schaefer, A. R. Spectral Response Self-Calibration and Interpolation of Silicon Photodiodes. *Appl. Opt.* **1980**, *19*, 3795−3799.
(36) Soci, C.; Zhang, A.; Xiang, B.; Dayeh, S. A.; Aplin, D. P. R.; Park, J.; Bao, X. Y.; Lo, Y. H.; Wang, D. ZnO Nanowire UV Photodetectors with High Internal Gain. *Nano Lett.* **2007**, *7*, 1003−1009.
(37) Peng, L.; Zhai, J. L.; Wang, D. J.; Wang, P.; Zhang, Y.; Pang, S.; Xie, T. F. Anomalous Photoconductivity of Cobalt-Doped Zinc Oxide Nanobelts in Air. *Chem. Phys. Lett.* **2008**, *456*, 231−235.
(38) Chen, Y. J.; Zhu, C. L.; Cao, M. S.; Wang, T. H. Photoresponse of SnO_2 Nanobelts Grown In Situ on Interdigital Electrodes. *Nanotechnology* **2007**, *18*, 285502.

(39) Zhang, D.; Li, C.; Han, S.; Liu, X.; Tang, T.; Jin, W.; Zhou, C. Ultraviolet Photodetection Properties of Indium Oxide Nanowires. *Appl. Phys. A: Mater. Sci. Process.* **2003**, *77*, 163−166.
(40) Liu, K.; Sakurai, M.; Liao, M.; Aono, M. Giant Improvement of the Performance of ZnO Nanowire Photodetectors by Au Nanoparticles. *J. Phys. Chem. C* **2010**, *114*, 19835−19839.